Frontiers in Scientific Research and Technology

Online ISSN: 2682-2970
Print ISSN: 2682-2962
http://fsrt.journals.ekb.eg

FSRT J 11 (2025) 101 - 114 10.21608/fsrt.2025.383591.1165

Mineralogical Characterization and Physical Beneficiation of Mineralized Lamprophyre Dykes from Wadi Nugrus-Abalea, Eastern Desert, Egypt

Mai M. Fathy[1], Gehad M. Saleh[1], Sherif Kharbish[2], Mohamed S. Kamar[1], Ali Maged[2,*], Mona M. Fawzy[1]

[1] Nuclear Materials Authority. P.O. Box 530, Maadi, Cairo, Egypt

[2] Geology Department, Faculty of Science, Suez University, 43221 Suez, Egypt

ARTICLE INFO

Article history:
Received 10 May 2025
Received in revised form 5 June 2025
Accepted 10 June 2025
Available online 14 June 2025

Keywords
Lamprophyre dykes,
Wadi Nugrus,
Polymetallic minerals,
Gravity,
Magnetic,
Eastern Desert,
Egypt.

ABSTRACT

This study investigates the mineralogical composition of two lamprophyre dykes located in the Wadi Nugrus-Abalea area, Egypt. Analysis revealed that the primary mineral constituents of the samples are quartz, feldspar, and muscovite, comprising approximately 79.2 wt.%. Additionally, the samples contain significant amounts of economically valuable polymetallic minerals—14.28 wt.% in the first dyke and 5.79 wt.% in the second. The altered lamprophyre samples were characterized using X-ray diffraction (XRD), X-ray fluorescence (XRF), and scanning electron microscopy (SEM), alongside analysis of their physical properties. Based on these results, flow sheets were proposed to outline the sequential physical beneficiation steps, including wet gravity separation followed by dry high-intensity magnetic separation, to concentrate valuable minerals and remove associated gangue. The study identified several industrially and strategically important polymetallic minerals within the lamprophyre samples, such as base metal minerals, kasolite that contains uranium (U), which consider a principal fuel for nuclear power generation as well as used to produce isotopes essential for medical diagnostics and cancer treatments, fluorite, chernovite-Y, and xenotime that has Rare Earth Elements (REEs) which play crucial roles in electronics, as well as iron oxides and base metals like copper that play an essential role for electrical wiring, electronics, and power generation and finally; zinc which a key role in galvanizing steel to prevent corrosion. Physical beneficiation processes successfully yielded high-grade mineral concentrates suitable for use as feedstock in chemical extraction processes, highlighting their potential for various industrial applications.

1. Introduction

Lamprophyre rocks are genetically associated with ultramafic, mafic, or intermediate magmatic compositions and typically intrude the continental crust at shallow levels, forming dykes and/or sills. They are characterized by a porphyritic texture, with phenocrysts of mafic minerals and apatite embedded in a fine-grained groundmass that often includes alkali feldspar and/or plagioclase. These rocks represent a distinctive petrographic group due to their mineralogical composition and volatile-rich nature.

At Wadi Nugrus in the Eastern Desert of Egypt, two ENE–WSW trending lamprophyre dykes have been identified, intruding porphyritic biotite granites. These dykes range from 0.5 to 1.5 meters in thickness and extend up to 3 kilometers in length. The lamprophyres are significantly altered and display prominent porphyritic textures, with plagioclase, olivine, and augite as major porphyritic constituents within a groundmass of similar mineralogy.

Notably, rounded to sub-rounded zoned ocelli with radiating or brush-like textures are common, serving as physical traps for mineralization.

Microscopic investigations reveal that these lamprophyres host a variety of economically important minerals, including base metal minerals, kasolite, chernovite-Y, fluorite, and xenotime, alongside iron oxides and base metals such as copper and zinc. While most basic dykes in Egypt's Precambrian terrane are considered non-mineralized and of limited exploration interest, the lamprophyre dykes at Wadi Nugrus are an exception. They appear to act as both geochemical and physical traps, playing a significant role in the remobilization and concentration of uranium (U), rare earth elements (REEs), and several base metals (e.g., Zn, W, Pb, Ag, Ni, Au, and Cu), especially in association with cataclastic zones trending NNW–SSE and E–W (Ibrahim et al., 2006; 2007; and 2010).

Given the polymetallic and mineralogically diverse nature of the lamprophyre dykes at Wadi Nugrus, physical beneficiation techniques play a crucial role in the concentration and separation of valuable minerals from

* Corresponding author at Suez University
E-mail addresses: Ali.Maged@suezuni.edu.eg (Ali Maged)

gangue. Due to the fine-grained and complex intergrowth of minerals, a combination of wet gravity separation and dry high-intensity magnetic separation was employed to enhance mineral recovery. Wet gravity methods effectively separate heavy minerals based on density differences, concentrating economically significant phases such as xenotime and fluorite (Masoud et al., 2012; Abd El Moneam et al., 2014; Raslan and Fawzy 2018; Fawzy et al., 2020; Fawzy et al., 2021; and Raslan et al., 2021)). Subsequently, magnetic separation techniques allow for the refinement of these concentrates by isolating magnetic and paramagnetic phases, including iron oxides and base metal-bearing minerals (Fawzy et al., 2021 and Raslan et al., 2021). This integrated beneficiation approach not only improves the grade of recovered materials but also enhances their suitability as feedstock for subsequent chemical processing and metal extraction, thereby supporting the economic viability of lamprophyre-hosted mineralization in this region (Fawzy et al., 2021 and Fawzy, 2021). In this study, the mineralogical characteristics and ore potential of the lamprophyres were analyzed in conjunction with physical beneficiation techniques to better understand ore evolution and mineralization processes in the Wadi Nugrus area.

2. Geologic setting

The Abu Rusheid area is situated approximately 45 km southwest of Marsa Alam in Egypt's Southeastern Desert and spans an area of about 3.0 km². The study site lies on the periphery of the extensive Abu Rusheid mineralized zone and is geographically bounded by longitudes 34° 45′ 45″ to 34° 46′ 34″ E and latitudes 24° 37′ 47″ to 24° 38′ 46″ N (Fig. 1). The Precambrian tectono-stratigraphic framework of the region (refer to Fig. 1) comprises several lithological units, including: (a) ophiolitic mélange, (b) gneissic rocks, (c) monzogranites, and (d) post-granitic dykes and veins—specifically lamprophyres (Ibrahim et al., 2004; and Fawzy et al., 2021).

The gneissic units are intersected by two prominent NNW–SSE trending shear zones. Along fractures within the lamprophyre dykes, mineralization is evident in the form of thin films containing uranium minerals, iron oxides, zinc, clay minerals, fluorite, and manganese oxides (Ibrahim et al., 2006 and 2007). The first shear zone, located near West Abu Rusheid, manifests as a V-shaped trench approximately 800 meters long and 5–20 meters wide. Geochemical trends across this zone indicate a decrease in uranium content toward the southern segment and a corresponding increase in aluminum oxide (Al_2O_3) and iron. Conversely, the northern segment is characterized by higher concentrations of uranium and copper mineralization. Leaching and alteration processes have resulted in the development of vugs, commonly filled with calcite, quartz, and uranium-bearing minerals, particularly near the lamprophyre intrusions.

The second shear zone, running parallel to the first, is about 280 meters long and varies between 2 to 10 meters in width. The rocks within these zones are typically fine- to medium-grained, heavily brecciated, and exhibit a diverse color spectrum, ranging from black and whitish to pink and red, attributable to intense metasomatic alterations. These include kaolinization, silicification, fluoridation, hematitization, and greisenization. Notably, greisenization is pronounced along the contacts between the gneissic rocks, ophiolitic mélange, and lamprophyres, as evidenced by the presence of banded muscovite-rich assemblages.

3. Sample Preparation and Analytical Methods

Six representative bulk samples, each weighing approximately 10 kg, were collected from two mineralized lamprophyre dykes located in the Wadi Nugrus–Abalea area. These samples were selected to be representative of the mineralogical variability within the dykes and were used for subsequent mineralogical and beneficiation studies. Initially, all samples were subjected to comminution to reduce particle size to below 1 mm. This process involved primary crushing using a jaw crusher, followed by grinding with a Denver rod mill. The ground material (-1.0 mm) was then subjected to desliming using a desliming cone to separate and quantify the slime fraction. Following desliming, the remaining material was classified into six particle size fractions (1000, 750, 500, 250, 125, and 53 µm) using a standard sieve series. These size fractions served as feeds for both mineralogical investigations and physical beneficiation processes.

For mineralogical analysis, approximately 100 g of each size fraction and a representative subsample from the bulk (unsieved) material were subjected to heavy liquid separation using bromoform (specific gravity = 2.89 g/cm³). This allowed for determining the total heavy mineral content and light gangue content across the size fractions and the bulk sample. The separated heavy and light fractions were thoroughly washed with acetone, dried, and weighed to calculate their respective percentages.

From the heavy mineral concentrates, monomineralic grains were hand-picked under a binocular microscope for detailed mineralogical characterization. Selected grains were analyzed using Scanning Electron Microscopy (SEM), X-ray Fluorescence (XRF), and X-ray Diffraction (XRD) techniques, all conducted at the Nuclear Materials Authority (NMA).

SEM analysis was performed using a Philips XL 30 system equipped with an Energy Dispersive Spectroscopy (EDS) unit. Operating conditions included an accelerating voltage of 30 kV, a beam diameter of 1 µm, and a counting time of 60–120 seconds. The minimum detectable concentration ranged from 0.1 to 1 wt.%. XRD analysis was conducted using a Bruker D8 Discover X-ray diffractometer with a copper Kα radiation source (λ = 1.541 Å), operating at 40 kV and 40 mA. Diffraction data were collected in reflection mode, over a 2θ range of 5° to 80°, with a step size of 0.05°.

All collected lamprophyre samples were initially ground to a particle size of less than 500 µm to enhance mineral liberation and facilitate separation. Due to the difference in specific gravity between the gangue and heavy economic minerals, the ground material was first subjected to wet gravity separation using a Wilfley shaking table (Model No. 13). This method was employed to concentrate the heavy

mineral fraction and remove the associated light silicate gangue as effectively as possible.

Following gravity separation, the obtained heavy fractions underwent dry high-intensity magnetic separation according to the difference of magnetic behavior of concentrated minerals using a Carpco magnetic separator (DHIMS, Model MIH (13) III-5). This step enabled the separation of paramagnetic minerals (magnetic fraction) from diamagnetic minerals (non-magnetic fraction). At the final stage, monomineralic grains were hand-picked from all processed fractions under a binocular microscope for subsequent mineralogical characterization and analysis.

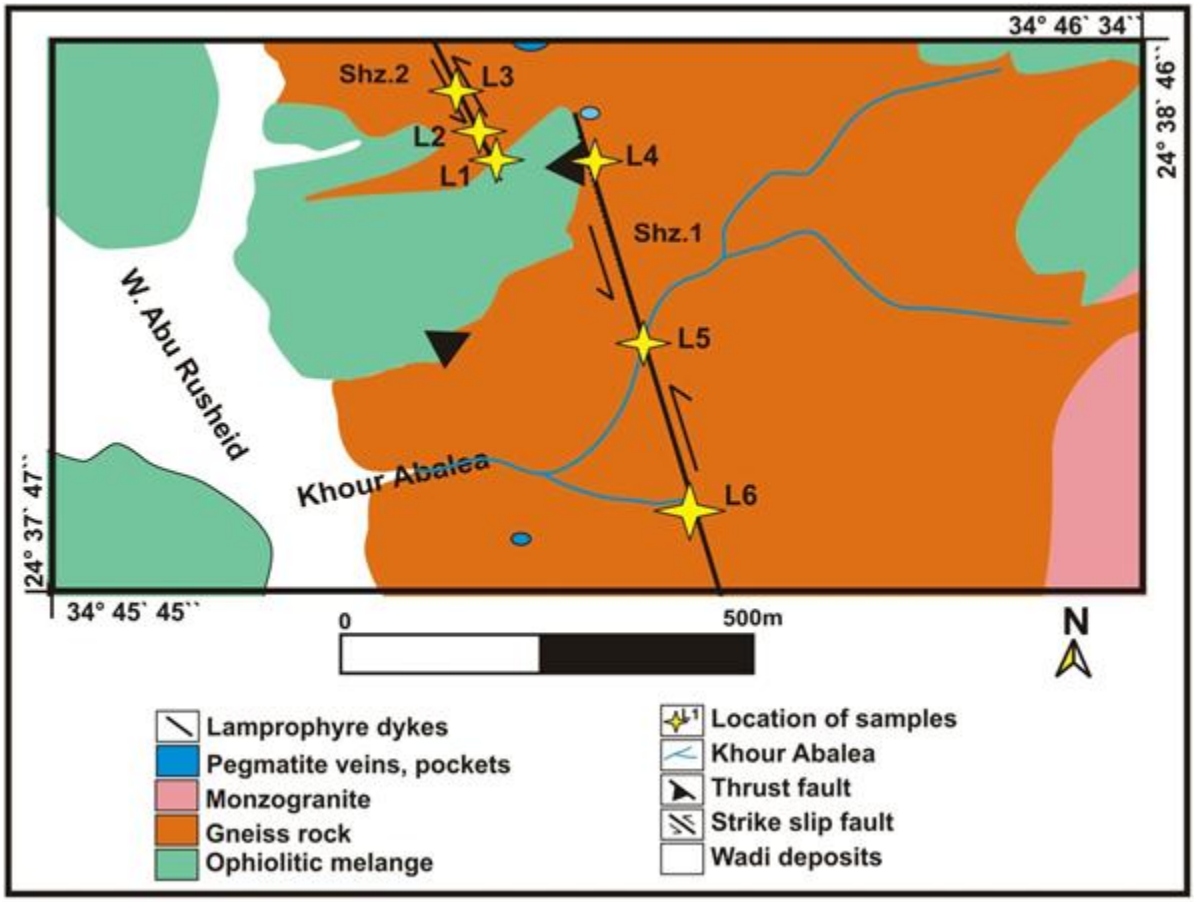

Figure 1. Detailed geologic map of Abu Rusheid area, Southeastern Desert, Egypt, after (Ibrahim et al., 2004).

4. Results and discussion

4.1 Grain Size Distribution and Heavy Mineral Assay

Grain size distribution analysis and cumulative percent passing data are presented in Tables 1 and 2 and illustrated in Figure 2. The results indicate that the D80 and D50 values for the samples are approximately 0.83 mm and 0.45 mm, respectively. These findings confirm that the comminution process effectively achieved the target particle size distribution. Specifically, 93.48 wt.% of the first lamprophyre sample (L1) and 93.82 wt.% of the second sample (L2) were retained within the operational size range of -1.00 mm to +0.053 mm. The generation of ultrafine material (slimes, <53 μm) was minimized to 6.52 wt.% and 6.18 wt.% for samples L1 and L2, respectively.

Tables 1 and 2 also present the distribution of total heavy minerals (specific gravity > 2.89) across various size fractions. The results show that 99.04% of the total heavy mineral content in L1 and 100% in L2 were recovered within the operational size range. This suggests that the applied grinding and sizing methods were highly efficient in preserving the economic mineral content. In terms of heavy mineral assay, the concentration in individual size fractions of sample L1 ranged between 3.54 wt.% and 24.63 wt.%, with a bulk average of 14.28%. For sample L2, heavy mineral content varied between 0.94 wt.% and 8.33 wt.%, averaging 5.79 wt.% in the bulk sample.

Microscopic examination of the heavy liquid separation products revealed that both samples are predominantly composed of quartz and feldspar. In sample L1, these gangue minerals constitute approximately 79.2 wt.%, while the heavy mineral content is 14.28 wt.%. For sample L2, quartz and feldspar make up about 88.03 wt.%, with heavy minerals accounting for 5.79 wt.%. These results highlight the potential for effective physical beneficiation of the studied lamprophyre samples. The significant concentration of heavy minerals within the operational size

range supports the feasibility of upgrading and recovering valuable mineral phases through gravity and magnetic separation techniques.

Table 1. Granulometric analysis and distribution of total heavy minerals across different size fractions of the first lamprophyre sample.

Grain size	Mass (%)	Comulative passing	HM(%)	HM distribution(%)
-1000:+750	28.41	100	24.63	49.03
-750:+500	18.36	71.59	13.58	17.48
-500:+250	20.93	53.22	12.58	18.45
-250:+125	12.06	32.29	12.64	10.68
-125:+53	13.72	20.24	3.54	3.40
Deslimed -1000:+53	93.48	-	-	99.04
Slimes (+53)	6.52	6.51	2.13	0.96
Origenal	100	0	14.28	100

Table 2. Granulometric analysis and distribution of total heavy minerals across different size fractions of the second lamprophyre sample.

Grain size	Mass (%)	Comulative passing	HM(%)	HM distribution(%)
-1000:+750	27.05	100	7.14	33.33
-750:+500	18.47	72.95	6.7	21.33
-500:+250	20.40	54.58	8.33	29.33
-250:+125	11.51	34.08	6.71	13.33
-125:+53	16.38	22.57	0.94	2.67
Deslimed -1000:+53	93.82	-	-	100
Slimes (+53)	6.18	6.18	-	-
Origenal	100	-	5.8	100

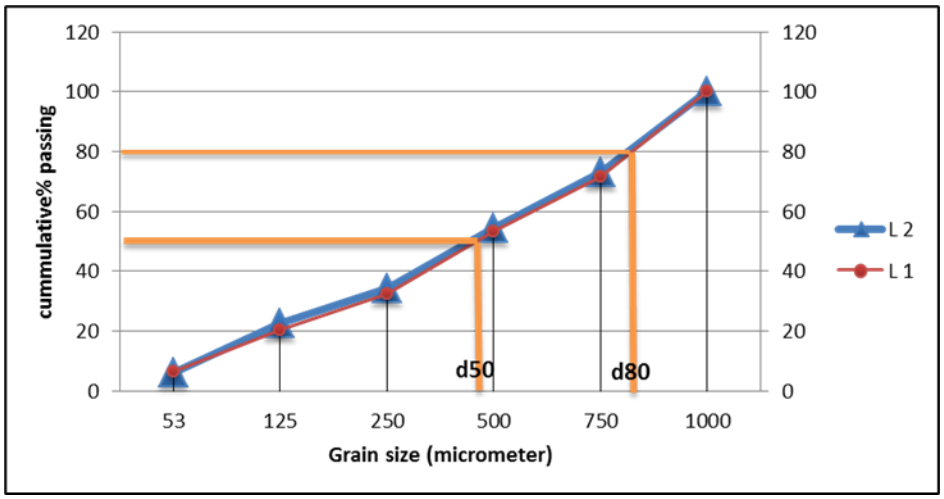

Fig. 2. Cumulative particle size distribution curves of the two lamprophyre samples studied.

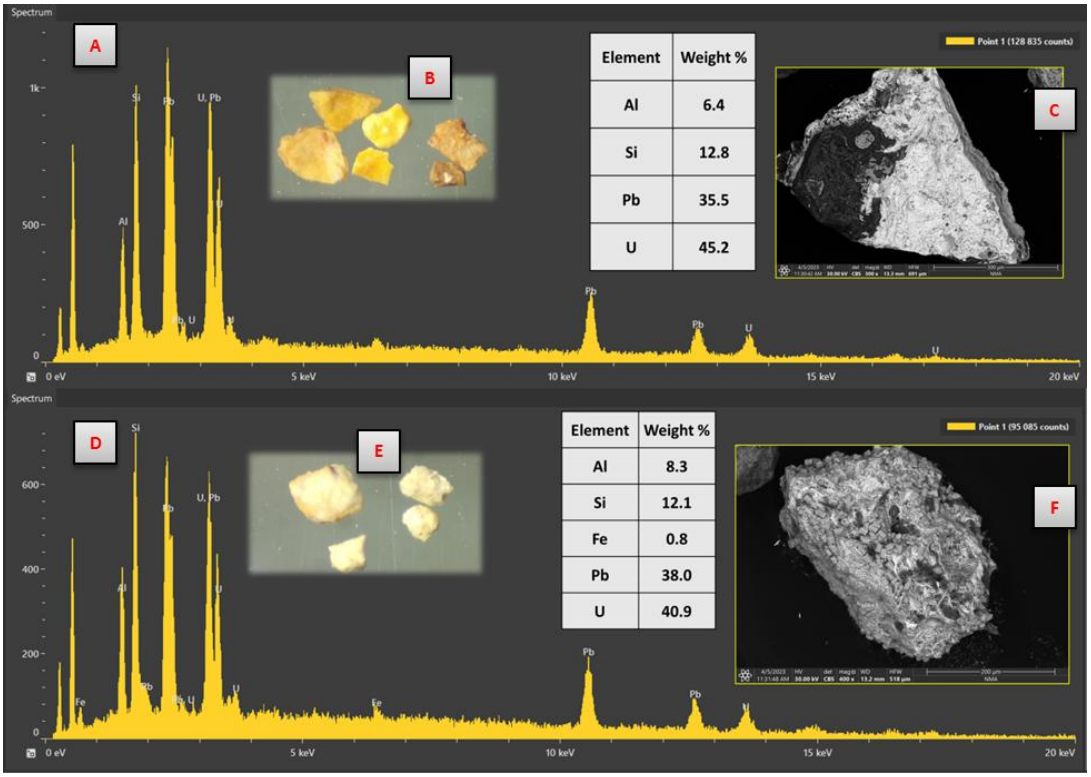

Fig. 3. Backscattered electron (BSE) images (c&f) and energy-dispersive X-ray (EDX) spectrum(a&d), along with stereo microscopic images of kasolite grains (b&e) showing their color, shape and the chemical composition of the grains.

4.2. Mineralogical Investigation

Kasolite: is a unique uranium silicate mineral that contains lead, making it easily distinguishable. In the lamprophyre samples, kasolite appears in aggregated crystal forms, ranging from rounded to sub-rounded shapes or as granular masses. Due to its relatively low hardness, the grains are primarily distributed in the finer fractions. The mineral is opaque with dull luster, as shown in the backscattered electron (BSE) image in Figure 3c&f. The color of kasolite varies, ranging from pale yellow to canary yellow and dark yellow Figure 3b&e.

Energy-dispersive X-ray (EDX) spectrum data for the studied kasolite, presented in Figures 3a&d, confirms that the mineral predominantly comprises lead, uranium, and silicon. Additionally, Figure 7 displays the XRD pattern of kasolite, identified with card no. 8-0297, further supporting the mineral's characterization.

Fluorite in the studied samples appears as large anhedral grains, exhibiting a range of colors from colorless to violet and pale green(Fig4b, e, & h). These grains are primarily distributed across various size fractions, with a notable concentration in the finer fractions, particularly those smaller than 0.5 mm. The backscattered electron (BSE) images (Fig4c, f, & i) and energy-dispersive X-ray (EDX) spectrum data(Fig4a, d, & g) provide detailed insights into the morphology and chemical composition of the fluorite grains.

The X-ray diffraction (XRD) pattern of the fluorite, displayed in Figures 7C and D, confirms its mineral identification with card number 75-0097, further validating the presence of fluorite within the sample and its distinct crystallographic characteristics.

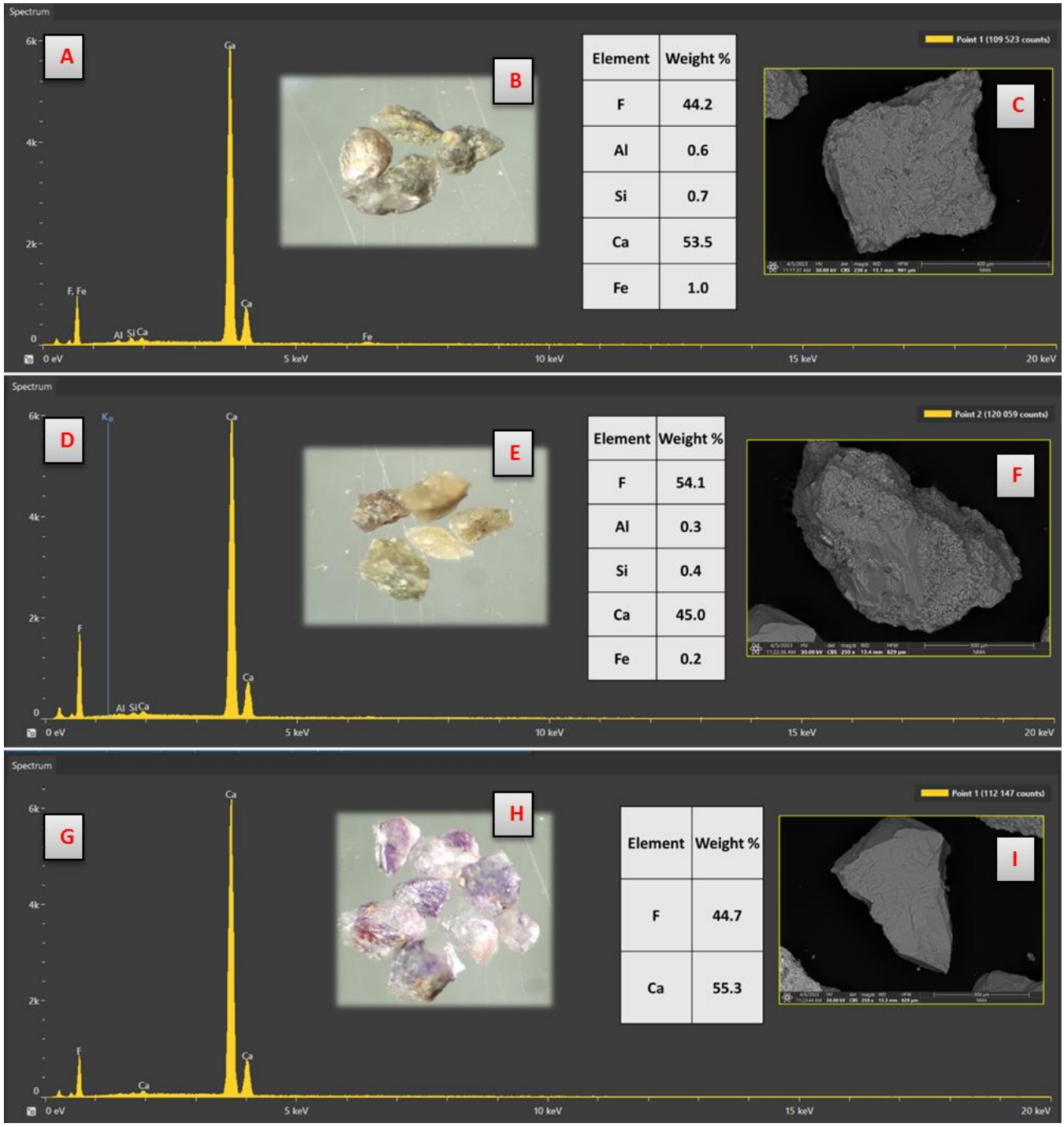

Fig. 4. BSE images(C, F, &I), EDX spectra(A, D, &G), and stereo microscopic images of fluorite grains(B, E, &H), highlighting their diverse colors, shapes, and chemical composition.

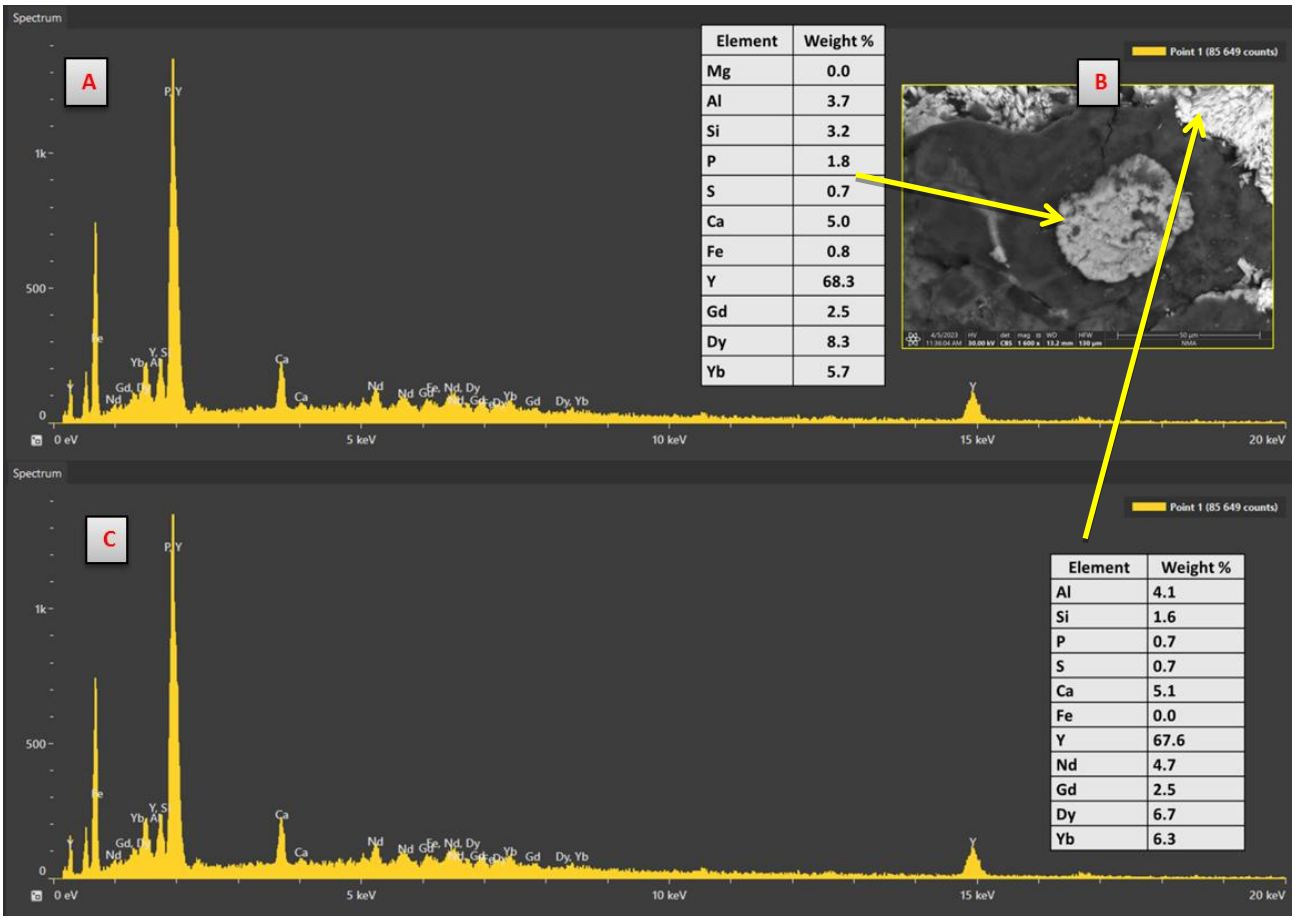

Fig.5. BSE images(B) and EDX spectra of xenotime inclusions (A&C).

Xenotime: is primarily found as inclusions within other mineral grains in the samples studied. Some of the xenotime grains show alteration, with inclusions of chernovite as a result of this process. The energy-dispersive X-ray (EDX) analysis of the xenotime grains is presented in Figure 5a&c. In addition to its yttrium content, xenotime commonly contains other heavy rare earth elements (HREEs), such as erbium, dysprosium, and yttrium. When the ytterbium (Yb) concentration exceeds that of yttrium, the mineral is classified as xenotime-(Yb). Some of the xenotime grains show alteration, with inclusions of chernovite due to this process.

The samples studied revealed various base metal mineralization distributed across all size fractions, characterized by dark brown to black coloration. SEM analyses identified manganese (Mn) and lead (Pb) as the primary constituents, with traces of zinc (Zn) and copper (Cu) (Fig.6). Additionally, BSE imaging and corresponding EDS spectra confirmed the presence of zircon, atacamite, barite, and xenotime in trace associations within the Abu Rushied lamprophyre dyke samples.

4.3. Chemical investigation

The chemical analyses of the two lamprophyre dyke samples (L1 and L2) from the Abu Rushied area are summarized in Table 3, and it reveal a composition rich in major oxides typical of mafic to intermediate igneous rocks. Both samples show high Fe_2O_3 contents, averaging 13.17% for L1 and 13.2% for L2, indicative of their ferromagnesian nature. TiO_2 is slightly higher in L2 (2.66%) than L1 (2.58%), while the P_2O_5 content remains low in both samples (around 0.19–0.197%). Both samples exhibit significant enrichment in terms of trace elements, rare earth elements (REEs), and radioactive elements. L1 is richer in ZnO (4066.67 ppm), CuO (3400 ppm), and PbO (7930 ppm) compared to L2 (ZnO: 4496.67 ppm, CuO: 3096.67 ppm, PbO: 6966.67 ppm). Y_2O_3 and Nb_2O_5 are similarly high in both samples, indicating consistent mafic affinity. REEs such as CeO_2 and La_2O_3 are notably more concentrated in L1 (739.67 ppm and 95.3 ppm, respectively) than in L2 (178.3 ppm and 58.33 ppm), while Nd_2O_3 appears only in L2 (299 ppm), reflecting either mineralogical differences or varying degrees of alteration. Uranium and thorium contents are elevated in both samples, with L1 showing higher U (1256.67 ppm) and L2 slightly enriched in Th (138.3 ppm). These elevated levels of U, Th, REEs, and base metals suggest the lamprophyres underwent significant hydrothermal activity and may have economic potential as sources of critical and radioactive elements.

4.4. Physical Processing

The mineralogical investigation of the lamprophyre samples studied, as summarized in Table 4, includes details of their mineral content, specific gravities, and magnetic properties. The results indicate that a significant proportion of the mineral assemblage consists of heavy minerals, accounting for approximately 14.28% by mass in sample L1 and 5.79% in sample L2. In contrast, light gangue minerals such as quartz and feldspar dominate the composition, representing about 79.2% in L1 and 88.03% in L2. This contrast in density suggests that simple wet gravity separation, such as on a shaking table, would be highly effective for concentrating the heavy fraction. Additionally, several heavy minerals in the samples, including xenotime, hematite, and base metals—exhibit paramagnetic properties, making them suitable for separation from diamagnetic minerals like kasolite and fluorite using a dry high-intensity magnetic separator (DHIMS).

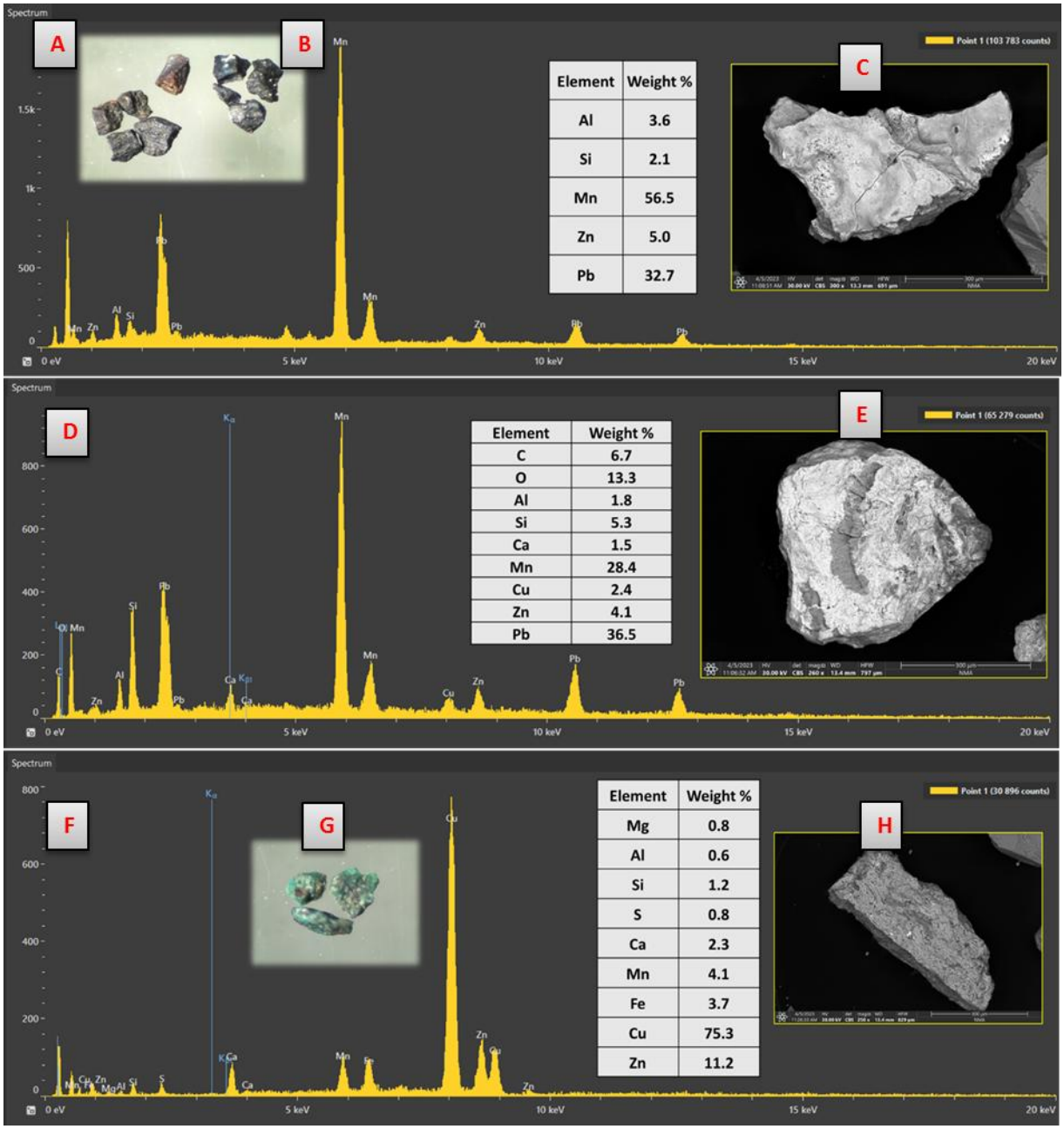

Fig. 6. BSE images and EDX spectra, along with stereo microscopic image of Pb-mineralization grains, illustrating their color, shape, and chemical composition (A, B, C, D, &E). Additionally, BSE images, EDX spectra, and stereo microscopic image of Cu-Zn mineralization grains, showing their color, shape, and chemical composition (F, G, &H).

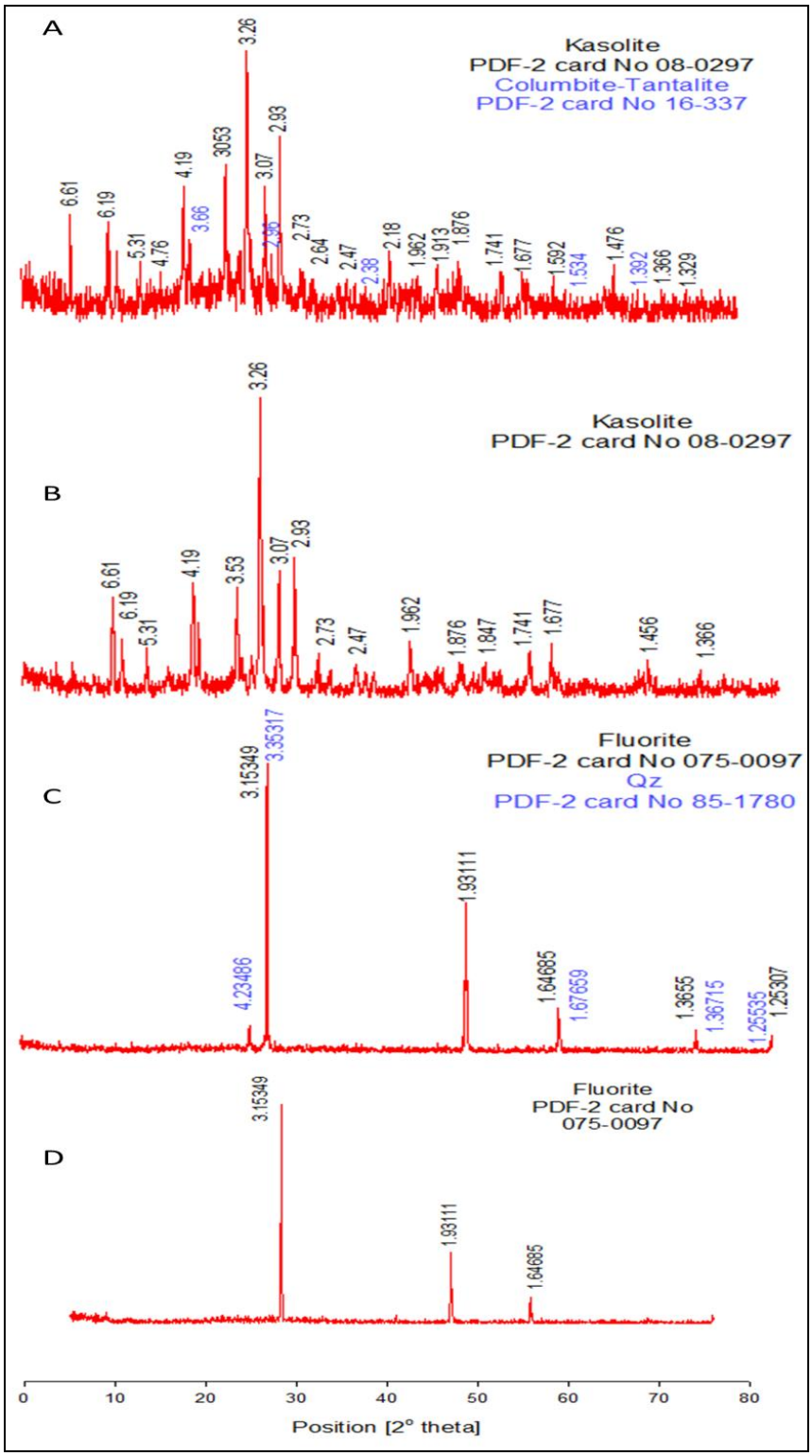

Fig.7. X-ray diffractogram of kasolite mineral (A&B) and Fluorite mineral (C&D).

4.4.1. Wet-gravity concentration

To obtain a clean concentrate of heavy minerals such as kasolite, fluorite, and other base metal minerals and to effectively separate them from the associated silicate gangue minerals (e.g., quartz and feldspar), a wet gravity separation process was employed using a Wilfley shaking table. The operation process was optimized under controlled conditions, including a feed rate of 5 kg/h, a water flow rate of 4 L/min, a stroke length of 10 mm, and a table inclination angle of 8°. The resulting heavy mineral concentrate and light gangue tailings were characterized using Scanning Electron Microscopy (SEM) and X-Ray Fluorescence (XRF). The separation and mineral identification results are presented in Figures 8, 9, and 10, and summarized in Table 5.

Table 3. Major and trace element analyses of three representative bulk samples from each lamprophyre dyke.

Sample Analysis	L1	L1	L1	Min	Max	Average	L2	L2	L2	Min	Max	Average
Fe_2O_3(ppm)	131000	132000	132000	131000	132000	131700	133000	133000	131000	131000	133000	132000
TiO_2(ppm)	25400	25500	26400	25400	26400	25800	26100	26700	26900	26100	26900	26600
P_2O_5(ppm)	1980	1920	2010	1920	2010	1970	1900	1900	19700	1900	19700	1900
ZnO (ppm)	33600	33900	33900	33600	33900	33800	22700	22900	22400	22400	22900	22700
CuO (ppm)	12800	13800	12600	12600	13800	13100	9700	9600	9600	9600	9700	9600
K_2O (ppm)	13000	13000	13100	13000	13100	13000	19000	18700	18800	18700	19000	18800
PbO (ppm)	7800	8080	7910	7910	8080	7930	7160	6950	6790	6790	7160	6967
Y_2O_3(ppm)	4650	4670	4690	4650	4690	4670	4960	4950	4680	4680	4960	4863
ZnO(ppm)	3950	4280	3970	3950	4280	4066.67	4350	4580	4560	4350	4560	4497
CuO(ppm)	3320	3470	3410	3320	3470	3400	3050	3220	3020	3020	3220	3097
Co_2O_3(ppm)	1230	1230	1290	1230	1290	1250	1350	1220	1230	1220	1350	1267
V_2O_5(ppm)	1130	1270	716	716	1270	1038.67	1100	1070	1110	1070	1110	1093
NiO (ppm)	1040	1040	1050	1040	1050	1043.3	1030	1010	1000	1000	1030	1013
Nb_2O_5(ppm)	868	854	892	854	892	871.3	906	887	827	827	906	873
Nd_2O_3(ppm)	-	-	-	-	-	-	543	354	-	-	543	299
CeO_2(ppm)	353	286	302	286	353	739.67	127	252	156	127	252	178
La_2O_3(ppm)	138	-	148	-	148	95.3	-	175	-	-	175	58
Ta_2O_3(ppm)	-	-	-	-	-	-	-	-	-	-	-	-
U(ppm)	1220	1260	1290	1220	1290	1256.67	1090	1130	1130	1090	1130	1116.67
Th (ppm)	118	121	122	118	122	120.3	115	146	154	115	154	138.3

The comparison between the elemental compositions of the original lamprophyre samples (L1 and L2) from the Abu Rushied area and their corresponding heavy mineral concentrates highlights important geochemical and beneficiation insights. The concentration factor, defined as the ratio of the element's content in the heavy concentrate to its content in the original sample, provides a clear measure of enrichment potential through physical separation techniques.

In both samples, certain major oxides such as Fe_2O_3 and TiO_2 show moderate enrichment in the heavy fractions, with concentration factors of 1.17 (Fe_2O_3) and 1.22 (TiO_2) for L1 and 1.19 (Fe_2O_3) and 1.21(TiO_2) for L2, reflecting their association with dense iron- and titanium-bearing minerals like hematite. In contrast, P_2O_5 and K_2O show concentration factors below unity in both samples, suggesting their association with lighter gangue minerals (e.g., feldspar or apatite) that are less responsive to gravity separation.

Among trace elements, PbO, ZnO, Nb_2O_5, and U exhibit the most significant enrichment in the heavy concentrates. For L1, ZnO demonstrates a remarkably high concentration factor of 7.9, and for L2, it reaches 5.05, indicating strong partitioning into heavy minerals, possibly Pb-Zn mineralization. Similarly, PbO is highly enriched (L1: 1.68, L2: 1.5), reinforcing its presence in dense phases. Uranium also shows a strong response, with concentration factors of 2.1 in L1 and 1.67 in L2, reflecting its association with heavy radioactive minerals such as kasolite. Nb_2O_5 shows moderate enrichment in both samples (L1: 1.24, L2: 1.282), consistent with its presence in high-density oxide minerals.

Table 4. Mineralogical composition of the lamprophyre samples, including nominal specific gravity and magnetic property data.

Lamprophyre samples mineral content	Specific gravity	Magnetic properties
Quartz	2.63–2.65	Diamagnetic
Feldspar	2.5–2.6	Diamagnetic
Muscovite	2.8–3.1	Paramagnetic
Kasolite	5.8–6.5	Diamagnetic
Fluorite	3.18	Diamagnetic
Hematite	3.55	Paramagnetic
Xenotime	4.4-5.1	Paramagnetic

Table 5. Major and trace element analyses of the original samples and their corresponding heavy concentrates obtained through tabling, along with the calculated concentration factors for each lamprophyre dyke sample**.**

Elemental Analyses	Original sample	Heavy concentrate	Concentration factor	Original sample	Heavy concentrate	Concentration factor
	L1			L2		
Fe_2O_3(%)	13.17	15.4	**1.17**	13.2	15.7	**1.19**
TiO_2(%)	2.58	3.13	**1.22**	2.66	3.23	**1.21**
P_2O_5(%)	0.197	0.177	0.898	0.19	0.164	0.86
K_2O (%)	1.3	1.39	1.1	1.88	1.84	0.98
PbO(PPM)	7930	13300	**1.68**	6966.67	10400	**1.5**
Y_2O_3(PPM)	4670	3970	0.85	4863.3	4640	0.95
ZnO (PPM)	4066.6	32100	**7.9**	4496.67	22700	**5.05**
CuO (PPM)	3400	3450	**1.01**	3096.67	3150	**1.02**
NiO (PPM)	1043.3	910	0.87	1013.3	1010	0.997
Nb_2O_5(PPM)	871.3	1080	1.24	873.3	1120	1.282
U(PPM)	1256.67	2610	**2.1**	1116.67	1860	**1.67**
Th (PPM)	120.3	120	0.99	138.3	120	0.87

Overall, the data suggests that gravity concentration is particularly effective in enriching elements like Zn, Pb, Nb, and U from the lamprophyre samples, while it is less effective for elements bound in lighter silicate minerals or those not preferentially hosted in heavy mineral phases. This highlights the beneficiation potential of Abu Rushied lamprophyres for select critical and economically valuable elements.

4.4.2. High Intensity magnetic separation.

Carpco High-Intensity Magnetic Separator is used to get two fractions from paramagnetic minerals (base metal and some iron minerals) and diamagnetic minerals (fluorite, kasolite, and some light grains); Fig11 shows flow sheet that illustrates the separation steps. The paramagnetic mineral products were executed at a medium air gap between the surface of the rotor and the magnetized pole of 1.5 mm. The speed of roll and the feed rate were controlled at 30 rpm and 100 g/ min respectively.

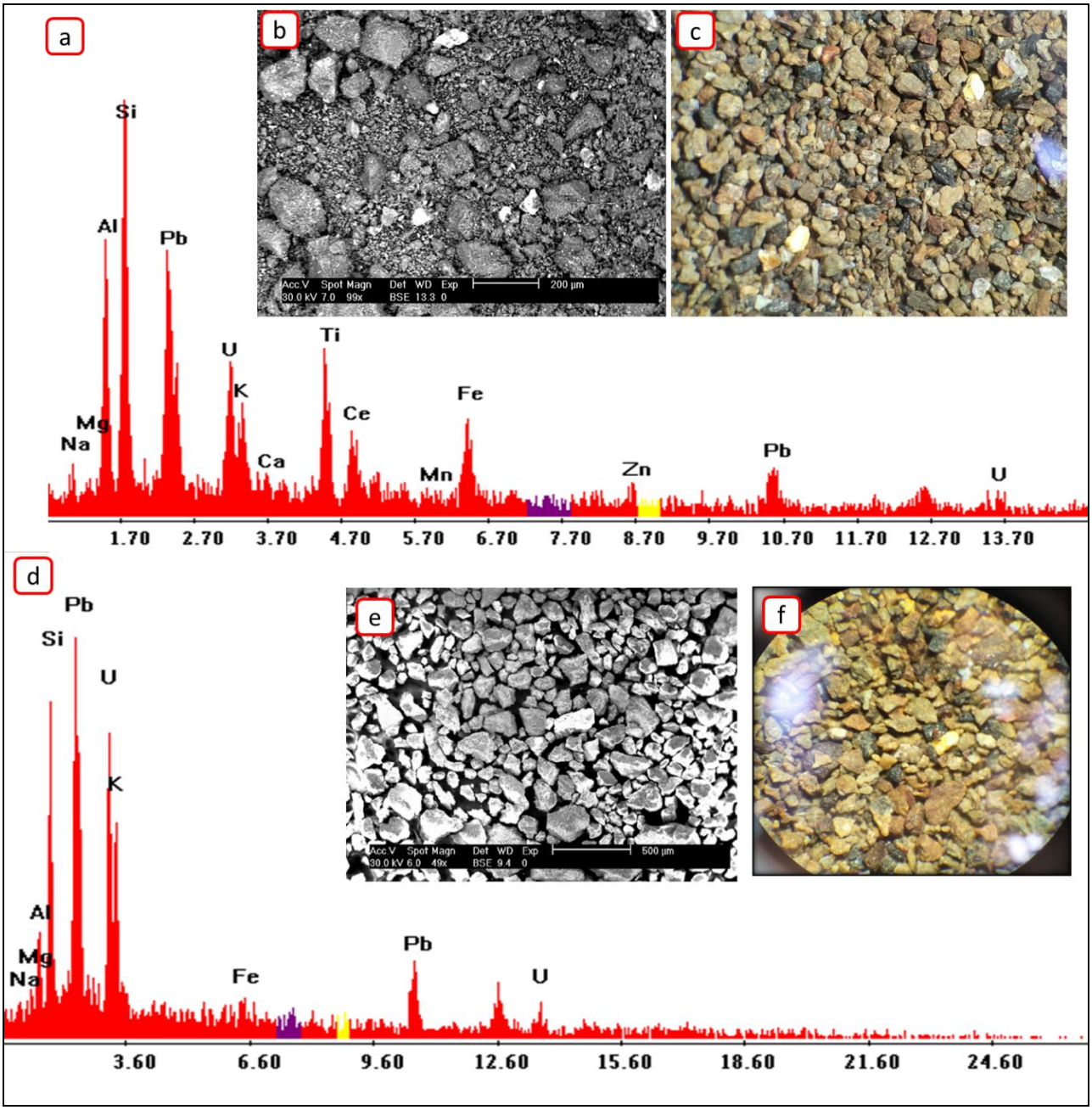

Fig. 8. EDS spectra (a, d), corresponding BSE images (b, e), and stereomicroscopic images (c, f) of heavy table concentrates from the Abu Rusheid lamprophyre dyke technology samples: L1 (a–c) and L2 (d–f).

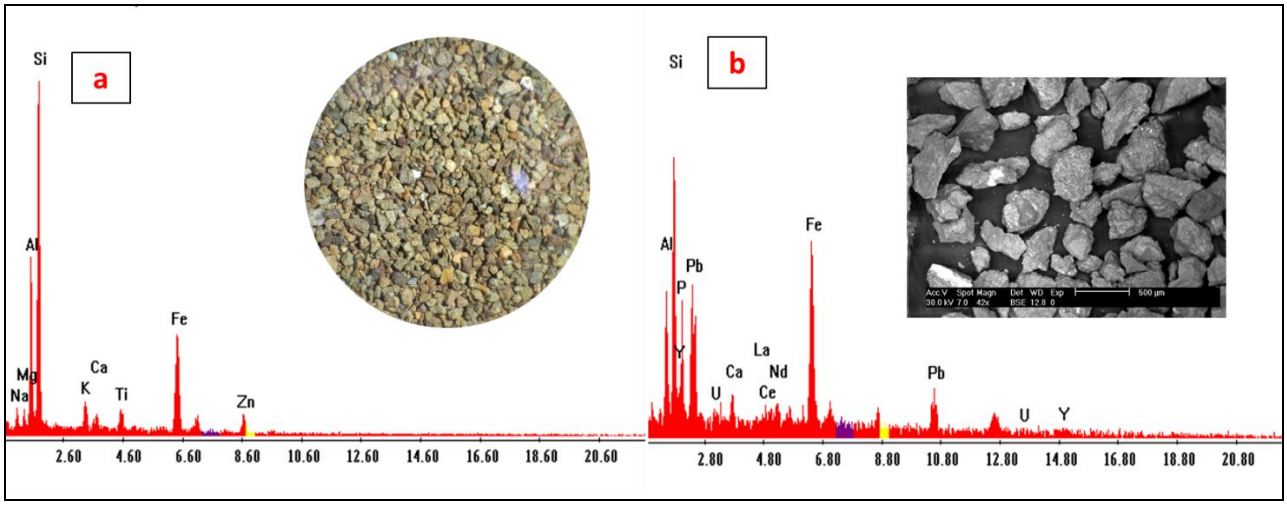

Fig.9. EDS spectra, corresponding BSE image, and stereomicroscopic image of light table fraction for the Abu Rusheid lamprophyre dyke technology samples L1, area scan a; spot analyses (b).

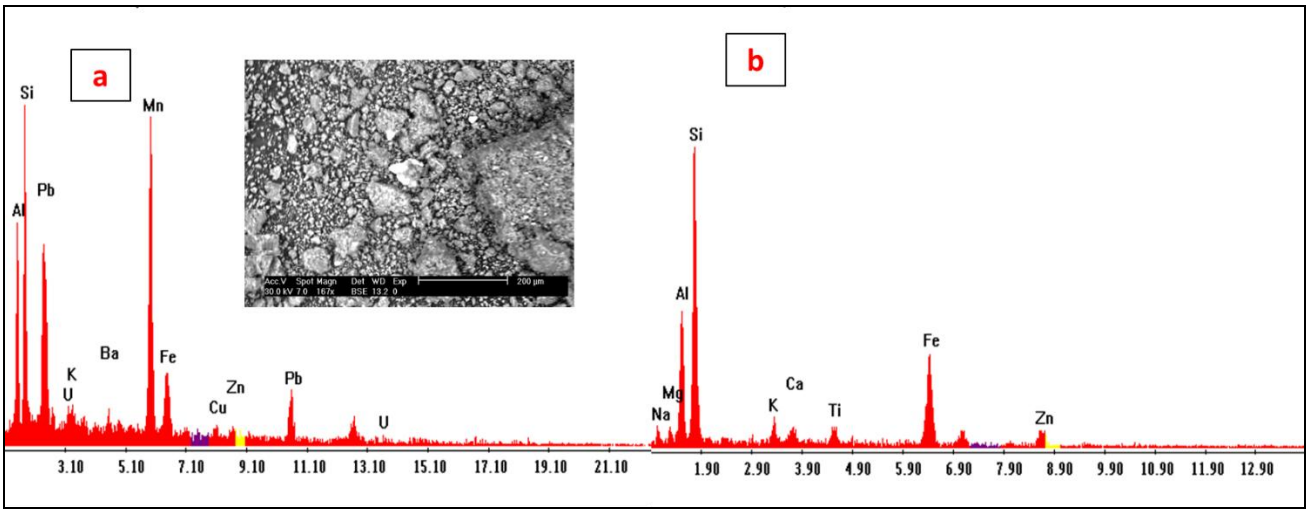

Fig.10. EDS spectra, corresponding BSE image, and stereomicroscopic image of slime fraction for the Abu Rusheid lamprophyre dyke technology samples L1, area scan a; spot analyses (b).

5. Conclusion

The lamprophyre dikes at the Wadi Nugrus–Abu Rusheid area represent a promising source of polymetallic mineralization, containing various economically and strategically significant minerals. Mineralogical analysis revealed that the first lamprophyre dike (L1) contains approximately 14.28% polymetallic minerals by mass, with 79.2% composed of gangue minerals such as quartz and feldspar. The second dike (L2) contains about 5.79% polymetallic minerals. Microscopic examinations using XRD and SEM confirmed the presence of valuable minerals including kasolite, base metal mineral, fluorite, and xenotime.

Physical beneficiation techniques, including wet gravity separation (shaking table), dry high-intensity magnetic separation, and flotation, were effectively applied. These methods enabled the effective removal of light gangue minerals (quartz and feldspar), separation of paramagnetic from diamagnetic heavy minerals, and concentration of kasolite from the diamagnetic fraction. As a result, three distinct concentrates were obtained: heavy paramagnetic concentrate, heavy diamagnetic concentrate, and kasolite-rich concentrate.

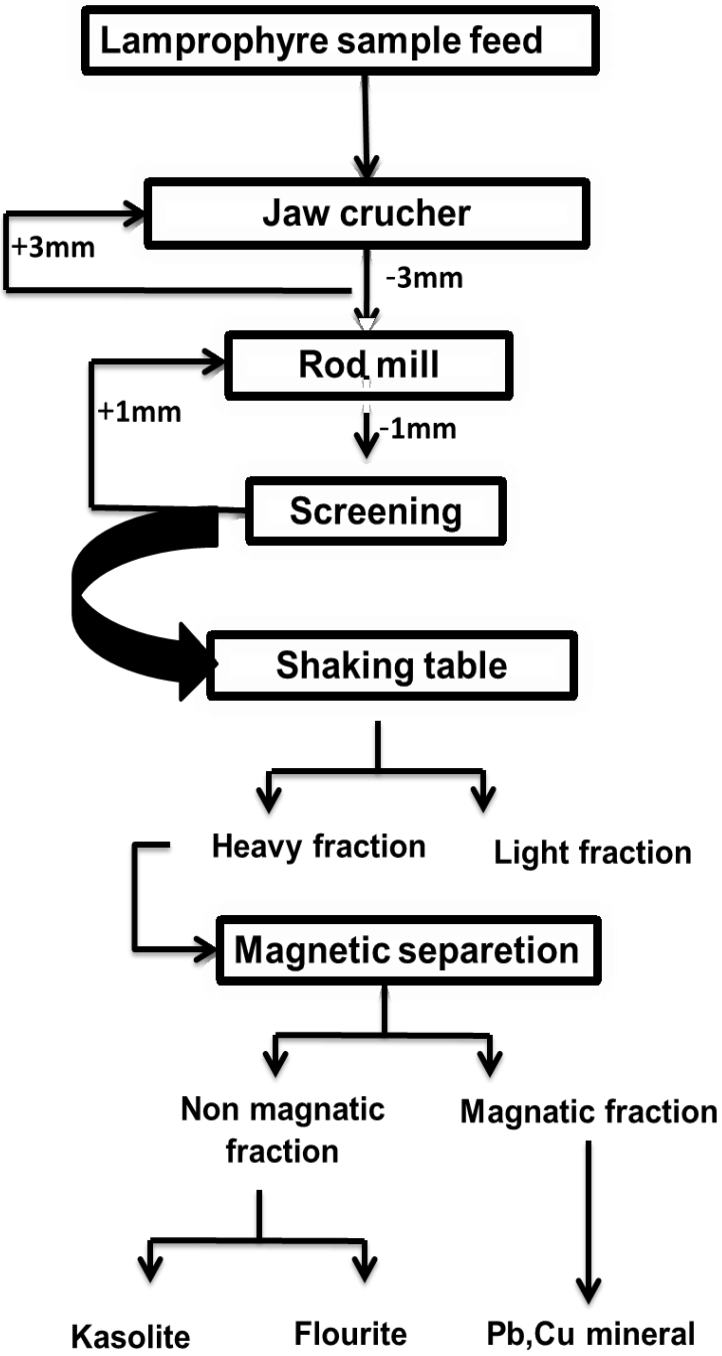

Fig.11. Preliminary process flow sheet proposed for separation of heavy minerals content from lamprophyre dyke samples.

References

Abd El Moneam, Y. K., Fawzy, M. M., Saleh, G. M., Abu El Soad, A. M., & Atrees, M. S. (2014). Comparative studies on flotation of kasolite using cationic and anionic surfactants. In *IJRET: International Journal of Research in Engineering and Technology*. http://www.ijret.org

Fawzy, M. (2021). Flotation separation of dravite from phlogopite using a combination of anionic/nonionic surfactants. *Physicochemical Problems of Mineral Processing*, 57(4), 87–95. https://doi.org/10.37190/ppmp/138587

Fawzy, M. M. (2018). Surface characterization and froth flotation of fergusonite from Abu Dob pegmatite using a combination of anionic and nonionic collectors. *Physicochemical Problems of Mineral Processing*, 54(3), 677–687. https://doi.org/10.5277/ppmp1865

Fawzy, M. M., Kamar, M. S., & Saleh, G. M. (2021). Physical processing for polymetallic mineralization of Abu Rusheid mylonitic rocks, South Eastern Desert of Egypt. *International Review of Applied Sciences and Engineering*, 12(2), 134–146. https://doi.org/10.1556/1848.2021.00200

Fawzy, M. M., Mahdy, N. M., & Sami, M. (2020). Mineralogical characterization and physical upgrading of radioactive and rare metal minerals from Wadi Al-Baroud granitic pegmatite at the Central Eastern Desert of Egypt. *Arabian Journal of Geosciences*, 13(11), 413. https://doi.org/10.1007/s12517-020-05381-z

Masoud M. S., Gharib M.E., Attaia G.E., Atrees M. S., Hassan M. A. And Fawzy M. M. (2012). Physical upgrading of uranium from El Sela kaolinized granite, South Eastern Desert, EGYPT. In *Egyptian Journal of Geology* (Vol. 56). https://www.researchgate.net/publication/352934399

Ibrahim ME, Abd El-Wahed AA, Rashed MA, Khaleal FM, Mansour GM, Watanabe K (2007). Comparative study between alkaline and calcalkaline lamprophyres in Abu Rusheid area, South Eastern Desert, Egypt. *The 10th International Mining, Petroleum, and Metallurgical Engineering Conference*, March 6–8: 99–115.

Ibrahim ME, El Tokhi MM, Saleh GM, Rashed MA (2006). Lamprophyre bearing-REEs South Eastern Desert, Egypt. *The 7th International Conference on Geochemistry*, Alexandria University, pp. 12–38.

Ibrahim ME, Saleh GM, Amer T, Mahmoud FO, Abu El Hassan AA, Ibrahim IH, Aly MA, Azab MS, Rashed MA, Khaleal FM, Mahmoud MA (2004). Uranium and associated rare metals potentialities of Abu Rusheid brecciated shear zone II, Southeastern Desert, Egypt. *(Internal report).*

Ibrahim, M.E., Saleh, G.M., Dawood, N.A., and Aly, G.M. (2010). Ocellar lamprophyre dyke bearing mineralization, Wadi Nugrus, Eastern Desert, Egypt: Geology, mineralogy and geochemical implications. *Journal of Geology and Mining Research*, 2(4), 74–86.

Raslan, M., & Fawzy, M. (2018). Mineralogy and Physical Upgrading of Fergusonite-Y and Hf-Zircon in The Mineralized Pegmatite of Abu Dob Granite, Central Eastern Desert, Egypt. *The Bulletin Tabbin Institute for Metallurgical Studies (TIMS)*, 107(1), 52–65. https://doi.org/10.21608/tims.2018.199447

Raslan, M. F., Kharbish, S., Fawzy, M. M., El Dabe, M. M., & Fathy, M. M. (2021). Gravity and Magnetic Separation of Polymetallic Pegmatite from Wadi El Sheih Granite, Central Eastern Desert, Egypt. *Journal of Mining Science*, 57(2), 316–326. https://doi.org/10.1134/S1062739121020162